

HARMONIC FORCED VIBRATION OF TWO ROTATING BLADES WITH FRICTION DAMPING

Vladimír Zeman, Miroslav Byrtus, Michal Hajžman*

This paper focuses on the modelling of harmonic vibration of two rotating blades affected by friction in contact of a rigid body placed in between the blade shroud. Harmonic blade excitation uniformly distributed in blade nodes in circumferential and axial direction is supposed. Flexible blades are discretized by FEM using 1D Rayleigh beam elements. The nonlinear friction forces in contact surfaces between the blade shroud and the friction element are taken into account using the harmonic balance method. Orbits of central contact points and dissipation energy are investigated in dependence on the excitation frequency. Dissipation energy amount in contact surfaces is confronted with blade tips vibration.

Keywords: blade vibration, friction damping, harmonic balance method

1. Introduction

Blades are the common and the most important parts in steam turbine design. With the increase of energy consumption, turbines are still innovated and the power of developed turbines is growing. On the other hand, it brings the greater complexity of newly produced energy systems and higher requirements on blades strength and fatigue. One of the main problems of the steam turbine is the high cycle fatigue failure of turbine blades due to blade vibration resonance in the operating range. Even if a machine is properly designed with respect to the excitation frequencies and turbine eigenfrequencies some excitation sources cannot be included in preliminary developments. Therefore the blades should be designed in such a way that they can absorb vibrations caused by unexpected or unusual excitation. Mathematical and computational models of blades and their systems are suitable tools for the investigation of their dynamical properties and for their optimization.

One of the most usual approaches to the suppression of undesirable blade vibrations is the employment of various friction effects. Detailed investigation of influences of friction on dynamical response of a simplified mechanical system represented by a beam can be found in [1]. Mainly the microslip phenomenon is discussed. Another method, which is analytical and is connected with non-spherical geometries, is developed in [2]. Many publications deal with the friction induced by means of underplatform (wedge) dampers. A method for the calculation of static balance supposing an in-plane motion of the wedge dampers is developed in [3]. An analytical approach is described in [4] and comparison of numerical simulation results with the results obtained by linearization is shown in [5]. A lumped model of bladed disk with dry friction dampers is presented in [6]. Nonlinear vibration is studied for both macro and micro-slip relative motions using describing functions and transforming

* prof. Ing. V. Zeman, DrSc., Ing. M. Byrtus, Ph.D., Ing. M. Hajžman, Ph.D., Department of Mechanics, Faculty of Applied Sciences, University of West Bohemia in Pilsen, Univerzitní 8, 306 14 Plzeň

nonlinear differential equations into nonlinear algebraic equations. The equivalent linearization method for the evaluation of linearized friction effects in blade dynamics represented by a very simple discrete mechanical system is discussed in [7]. In general, the equivalent linearization method can be used as a first approximation of the influence of friction by so-called equivalent viscous damping [8]. Also, experimental methods for the evaluation of friction significance in the problems of blade vibrations are very important. Some comparison of experimental and theoretical analysis is shown in [9], pure experimental results are described in [10] and the influences of temperature are experimentally investigated in [11].

In case of turbine blades, main excitation source is harmonic with nozzle frequency, which is given by a product of rotational frequency of bladed disk and the number of stator blades [12]. Therefore, one can assume the steady-state dynamic response to the mentioned excitation as a single-frequency harmonic oscillating motion. In consequence of spatial motion of blade shrouds linked by friction bodies (dampers), relative (slip) motion of contact points in contact surfaces which have approximately elliptic trajectories (orbits). The development of methodology focused on the investigation of influence of friction forces, friction element shape and angular velocity of rotating blades on orbits of contact points, energy dissipation and blade vibration suppression are points of the presented paper.

2. Methodology of two rotating blades with friction damper modelling

Let us consider a system of two blades fixed with a rigid disk rotating with angular velocity ω . A friction element with inclined planar contact surfaces a and b is wedged in between the blade shroud (Fig. 1). As a simplification, the contacts of the friction element and the blade shrouds are concentrated to point B in plane $b \equiv \widehat{\xi_B \eta_B}$ and to point A in plane $a \equiv \widehat{\xi_A \eta_A}$, respectively.

Blades are modelled as 1D continuum discretized by beam elements with uniformly distributed nodes along the axes of the blades. End nodes C_1 and C_2 of the blades are fixed with the rigid blade shroud. As the blades rotate, the centrifugal force $m_D r_D \omega^2$ pushes the friction element towards contact surfaces a and b of the adjacent blade shroud. The friction element acts on blades by normal forces N_A and N_B and by friction forces $\vec{T}_A(T_{A\xi}, T_{A\eta})$ and $\vec{T}_B(T_{B\xi}, T_{B\eta})$. Let us suppose, the blades are excited by harmonic forces with frequency $\omega_k = k\omega$ acting in tangential and axial (parallel to axis of rotation) direction. Excitation forces are uniformly concentrated in nodes along the blades.

Equations of motion of blades with shroud and friction element can be expressed in rotating local coordinate systems x_j, y_j, z_j , $j = 1, 2$ (blades) and x_D, y_D, z_D (friction element), where x_j and x_D are identified with axis of the blades and with radial of friction element. Axes y_j, y_D are parallel with fixed axis of disk rotation y_f (Fig. 1). In generalized coordinates

$$\mathbf{q}_j = [\dots u_i, v_i, w_i, \varphi_i, \vartheta_i, \psi_i, \dots]_j^T, \quad j = 1, 2. \quad (1)$$

expressing displacements in axis directions and angular displacements about them in nodes $i = 1, \dots, N$ of the blade with shroud considering excluded friction element, equations of motion have the form [13]

$$\mathbf{M}_B \ddot{\mathbf{q}}_j + (\omega \mathbf{G}_B + \mathbf{B}_B) \dot{\mathbf{q}}_j + (\mathbf{K}_{s,B} - \omega^2 \mathbf{K}_{d,B} + \omega^2 \mathbf{K}_{\omega,B}) \mathbf{q}_j = \mathbf{f}_{\omega,B} + \mathbf{f}_B(t), \quad (2)$$

where symmetric matrices of order $6N$ \mathbf{M}_B , \mathbf{B}_B , $\mathbf{K}_{s,B}$, $\mathbf{K}_{d,B}$, $\mathbf{K}_{\omega,B}$ are mass, material damping, static stiffness, softening under rotation and bending stiffening under rotation,

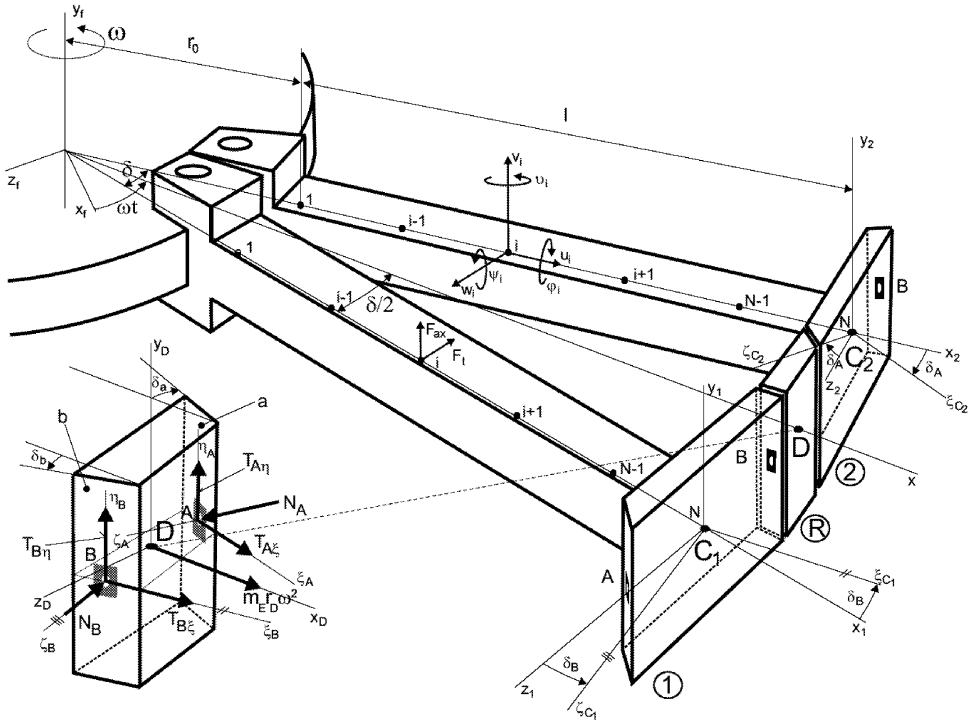


Fig.1: Two rotating blades with friction element

respectively. Matrix $\omega \mathbf{G}_B$ is a skew symmetrical matrix of gyroscopic effects. Constant centrifugal forces are expressed by vector $\mathbf{f}_{\omega, B}$ and hydrodynamical forces caused by vapour flow through fixed nozzles. Based on the analysis of vapour pressure field [14], hydrodynamic forces can be approximately expressed in a blade model (2) as a superposition of vectors of constant mean forces $\mathbf{f}_{B,0}$ and harmonic variable components with nozzle frequency $\omega_k = k\omega$ as follows

$$\mathbf{f}_B(t) = \mathbf{f}_{B,0} + \mathbf{f}_B \cos \omega_k \left(t + \frac{\delta_j}{\omega} \right), \quad j = 1, 2, \quad \delta_1 = 0, \quad \delta_2 = \delta, \quad (3)$$

where δ represents pitch angle of blades.

In generalized coordinates

$$\mathbf{q}_D = [u, v, w, \varphi, \vartheta, \psi], \quad (4)$$

the equations of motion of still isolated rigid friction element can be written in the matrix form analogous to the blade model

$$\mathbf{M}_D \ddot{\mathbf{q}}_D + \omega \mathbf{G}_D \dot{\mathbf{q}}_D - \omega^2 \mathbf{K}_{d,D} \mathbf{q}_D = \mathbf{f}_{\omega, D}. \quad (5)$$

After placing the friction element in between the blade shroud, acting of contact elastic and friction forces is concentrated into contact points *A* and *B*. Linearized model of blades connected by means of friction element will be further expressed by using perturbation displacements, which define blade and friction element displacements from static equilibrium given by centrifugal forces and by mean values of hydrodynamical forces. Contact viscous-elastic and friction forces are then replaced by forces transmitted by springs and dampers

with equivalent viscous damping, which are calculated under assumption of constant normal forces $N_{X,0}$. These forces are calculated from static equilibrium condition of friction element

$$N_{X,0} = m_D r_D \omega^2 \frac{\cos \delta_X}{\sin(\delta_a + \delta_b)}, \quad X = A, B. \quad (6)$$

Angles of contact surfaces skewing between blade shroud and friction element are displayed in Fig. 1.

In configuration space of perturbed generalized coordinates defined by vector

$$\mathbf{q} = [\mathbf{q}_1^T, \mathbf{q}_D^T, \mathbf{q}_2^T]^T, \quad (7)$$

equation of motion of the system is then written in the form

$$\mathbf{M} \ddot{\mathbf{q}} + (\omega \mathbf{G} + \mathbf{B} + \mathbf{B}_C + \mathbf{B}_e) \dot{\mathbf{q}} + (\mathbf{K}_s - \omega^2 \mathbf{K}_d + \omega^2 \mathbf{K}_\omega + \mathbf{K}_C) \mathbf{q} = \mathbf{f}(t). \quad (8)$$

In accordance with equation of motion (2) and (5), the below presented matrices have a block-diagonal structure

$$\begin{aligned} \mathbf{M} &= \text{diag}(\mathbf{M}_B, \mathbf{M}_D, \mathbf{M}_B), & \mathbf{G} &= \text{diag}(\mathbf{G}_B, \mathbf{G}_D, \mathbf{G}_B), \\ \mathbf{B} &= \text{diag}(\mathbf{B}_B, \mathbf{0}, \mathbf{B}_B), & \mathbf{K}_s &= \text{diag}(\mathbf{K}_{s,B}, \mathbf{0}, \mathbf{K}_{s,B}), \\ \mathbf{K}_d &= \text{diag}(\mathbf{K}_{d,B}, \mathbf{K}_{d,D}, \mathbf{K}_{d,B}), & \mathbf{K}_\omega &= \text{diag}(\mathbf{K}_{\omega,B}, \mathbf{0}, \mathbf{K}_{\omega,B}). \end{aligned} \quad (9)$$

Excitation vector

$$\mathbf{f}(t) = \left[\mathbf{f}_B^T \cos \omega_k t, \mathbf{0}, \mathbf{f}_B^T \cos \omega_k \left(t + \frac{\delta}{\omega} \right) \right]^T \quad (10)$$

is defined by vector of amplitudes of harmonic variable components of hydrodynamic forces

$$\mathbf{f}_B = [\dots, 0, F_{ax}, -F_t, 0, 0, 0, \dots]^T \quad (11)$$

acting at each blade node in axial and tangential direction (Fig. 1). The influence of contact viscous-elastic and friction forces is described by stiffness coupling matrix \mathbf{K}_C , damping matrix proportional to contact stiffness matrix $\mathbf{B}_C = \beta_C \mathbf{K}_C$ comprising the influence of contact damping in contact surfaces and by matrix of equivalent viscous damping \mathbf{B}_e respecting slip friction forces.

Coupling contact matrix can be derived from potential (deformation) energy

$$E_p^C = \frac{1}{2} \sum_{X=A,B} (k_X \zeta_X^2 + \varphi_X^T \mathbf{K}_X \varphi_X), \quad (12)$$

where k_X represents linearized translational contact stiffnesses [15] in normal direction of contact surfaces of blade shroud with friction element and elements of diagonal matrix $\mathbf{K}_X = \text{diag}(k_{\xi_X \xi_X}, k_{\eta_X \eta_X})$ correspond to rotational contact stiffnesses around axes ξ_X and η_X (Fig. 1). Relative displacements ζ_X in the normal direction are expressed by means of vectors of generalized coordinates \mathbf{q}_{C1} , \mathbf{q}_{C2} of end points of blades and by vector of generalized coordinates \mathbf{q}_D of friction element mass centre

$$\zeta_X = \zeta_{X,C_j}^T \mathbf{q}_{C_j} - \zeta_{X,D}^T \mathbf{q}_D, \quad (X = B \wedge j = 1) \vee (X = A \wedge j = 2) \quad (13)$$

where row vectors

$$\begin{aligned}\zeta_{B,C_1}^T &= [\sin \delta_B, 0, \cos \delta_B] [\mathbf{E} \mathbf{R}_{C_1,B}^T], \\ \zeta_{A,C_2}^T &= [-\sin \delta_A, 0, \cos \delta_A] [\mathbf{E} \mathbf{R}_{C_2,A}^T], \\ \zeta_{B,D}^T &= [\sin \delta_b, 0, \cos \delta_b] [\mathbf{E} \mathbf{R}_{D,B}^T], \\ \zeta_{A,D}^T &= [-\sin \delta_a, 0, \cos \delta_a] [\mathbf{E} \mathbf{R}_{D,A}^T]\end{aligned}\quad (14)$$

are determined by angles designated in Fig. 1 and by operators of cross product (symbol \mathbf{R}) defined by radius vectors of contact points $X = A, B$ in coordinate systems x_j, y_j, z_j with origins in end nodes of the blades and in coordinate system x_D, y_D, z_D with origin in centre D .

Vector φ_X of relative angular displacements of blade shroud with respect to friction element in (12) can be expressed using vectors of angular displacements $\varphi_j = [\varphi_j, \theta_j, \psi_j]^T$, $j = 1, 2$ of blade shrouds and friction element $\varphi_D = [\varphi_D, \theta_D, \psi_D]^T$

$$\varphi_A = \begin{bmatrix} \cos \delta_A & 0 & \sin \delta_A \\ 0 & 1 & 0 \end{bmatrix} \varphi_2 - \begin{bmatrix} \cos \delta_a & 0 & \sin \delta_a \\ 0 & 1 & 0 \end{bmatrix} \varphi_D, \quad (15)$$

$$\varphi_B = \begin{bmatrix} \cos \delta_B & 0 & -\sin \delta_B \\ 0 & 1 & 0 \end{bmatrix} \varphi_1 - \begin{bmatrix} \cos \delta_b & 0 & -\sin \delta_b \\ 0 & 1 & 0 \end{bmatrix} \varphi_D. \quad (16)$$

If the contact stiffness per unit area is assumed to be constant as well as the rectangle (real) contact area with sides a_{ef} , $h_{a,ef}$ (b_{ef} , $h_{b,ef}$), rotational contact stiffnesses around axes ξ_X and η_X are

$$k_{\xi_A \xi_A} = \frac{k_A}{12} h_{a,ef}^2, \quad k_{\xi_B \xi_B} = \frac{k_B}{12} h_{b,ef}^2, \quad k_{\eta_A \eta_A} = \frac{k_A}{12} a_{ef}^2, \quad k_{\eta_B \eta_B} = \frac{k_B}{12} b_{ef}^2. \quad (17)$$

Coupling stiffness matrix is then determined from the equivalence

$$\frac{\partial E_p^C}{\partial \mathbf{q}} = \mathbf{K}_C \mathbf{q}, \quad (18)$$

where vector \mathbf{q} of generalized coordinates was defined in (7).

3. Substitution of friction forces in contact surfaces with equivalent viscous damping

In consequence of harmonic excitation, the steady-state slip motion of contact point in direction of axis ξ_X , η_X is supposed to be harmonic

$$\begin{aligned}\xi_X(t) &= \xi_{X,C_j}^T \mathbf{q}_{C_j}(t) - \xi_{X,D}^T \mathbf{q}_D(t), \\ \eta_X(t) &= \eta_{X,C_j}^T \mathbf{q}_{C_j}(t) - \eta_{X,D}^T \mathbf{q}_D(t),\end{aligned}\quad (X = B \wedge j = 1) \vee (X = A \wedge j = 2). \quad (19)$$

Row transformation vectors transforming vectors of generalized coordinates of end blade nodes C_j and mass centre D of friction element into displacements of contact points $X = A, B$

$$\begin{aligned}\xi_{X,C_j}^T &= [\cos \delta_X, 0, \pm \sin \delta_X] [\mathbf{E} \mathbf{R}_{C_j,X}^T], \\ \xi_{X,D}^T &= [\cos \delta_x, 0, \pm \sin \delta_x] [\mathbf{E} \mathbf{R}_{D,X}^T], & \text{" + " for } X = A \wedge x = a, \\ \eta_{X,C_j}^T &= [0, 1, 0] [\mathbf{E} \mathbf{R}_{C_j,X}^T], & \text{" - " for } X = B \wedge x = b \\ \eta_{X,D}^T &= [0, 1, 0] [\mathbf{E} \mathbf{R}_{D,X}^T],\end{aligned}\quad (20)$$

are expressed using angles denoted in Fig. 1 and using operators of cross product defined by radius vectors of contact points X expressed in coordinate systems x_j, y_j, z_j whose origins are identical to points C_j regarding the blade shroud. Radius vector regarding the contact point at the friction element is expressed in coordinate system x_D, y_D, z_D with origin identical to point D . The radius vector of contact points in contact surfaces can be expressed in a complex form $\tilde{r}_X(t) = \xi_X(t) + i\eta_X(t)$, $X = A, B$.

Harmonic variable coordinates can be further expressed as real parts of their complex form

$$\tilde{\xi}_X(t) = \left(\xi_{X,C_j}^T \tilde{\mathbf{q}}_{C_j} - \xi_{X,D}^T \tilde{\mathbf{q}}_D \right) e^{i\omega_k t}, \quad \tilde{\eta}_X(t) = \left(\eta_{X,C_j}^T \tilde{\mathbf{q}}_{C_j} - \eta_{X,D}^T \tilde{\mathbf{q}}_D \right) e^{i\omega_k t}, \quad (21)$$

where $\tilde{\mathbf{q}}_{C_j}$ and $\tilde{\mathbf{q}}_D$ are vectors of complex amplitudes of nodal displacements. Obviously, it holds

$$\xi_X(t) = \bar{\xi}_X \cos \omega_k t - \overline{\xi}_X \sin \omega_k t, \quad \eta_X(t) = \bar{\eta}_X \cos \omega_k t - \overline{\eta}_X \sin \omega_k t, \quad (22)$$

where real (imaginary) parts of complex amplitudes of coordinates of contact points are labelled by one (two) overline. In consequence of harmonic variable displacements, the shape of contact points orbits is elliptical (see Fig. 2), given by major and minor semi-axes

$$a_X = \sqrt{\xi_X^2(t_1) + \eta_X^2(t_1)}, \quad b_X = \sqrt{\xi_X^2(t_2) + \eta_X^2(t_2)} \quad (23)$$

and by angles of major semi-axes which satisfy

$$\tan \delta_X = \frac{\eta_X(t_1)}{\xi_X(t_1)}, \quad X = A, B. \quad (24)$$

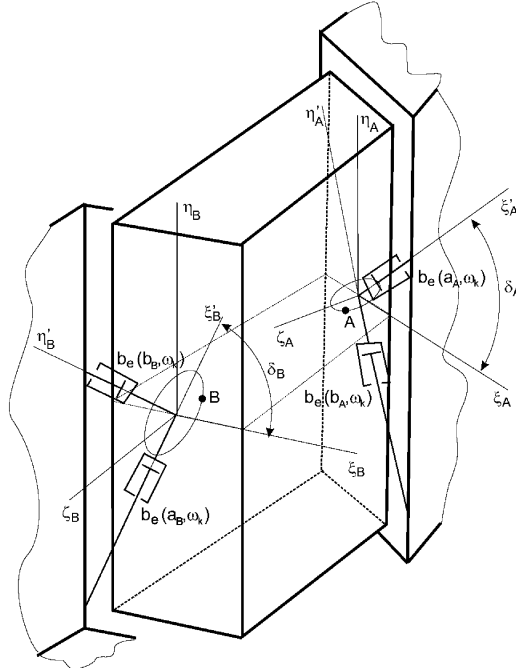


Fig.2: Elliptical trajectories of the contact points in contact surfaces

Time instants t_1 and t_2 correspond to extreme values of radius vectors which are calculated based on conditions of zero first-order derivative of radius vectors magnitudes. After rearrangement,

$$\omega_k t_1 = \frac{1}{2} \arctan \frac{2 \left(\bar{\xi}_X \bar{\xi}_X + \bar{\eta}_X \bar{\eta}_X \right)}{\bar{\xi}_X^2 + \bar{\eta}_X^2 - \bar{\xi}_X^2 - \bar{\eta}_X^2} \quad \text{and} \quad \omega_k t_2 = \omega_k t_1 + \frac{\pi}{2} \quad (25)$$

is obtained.

Based on experimentally verified theory [16], friction forces acting in contact surfaces can be approximately expressed by forces transmitted by viscous dampers placed in directions of semi-axes of the ellipse (Fig. 2)

$$\begin{bmatrix} T_{X\xi'} \\ T_{X\eta'} \end{bmatrix} = \begin{bmatrix} b_e(a_X, \omega_k) & 0 \\ 0 & b_e(b_X, \omega_k) \end{bmatrix} \begin{bmatrix} c_{X\xi'} \\ c_{X\eta'} \end{bmatrix}, \quad X = A, B \quad (26)$$

where

$$b_e(a_X, \omega_k) = \frac{4 f_x N_{X,0}}{\pi (a_X \omega_k)^p}, \quad b_e(b_X, \omega_k) = \frac{4 f_x N_{X,0}}{\pi (b_X \omega_k)^p} \quad (27)$$

are equivalent damping coefficients and $c_{X\xi'}$, $c_{X\eta'}$ are components of slip velocity in semi-axes directions. Friction coefficients f_a for $X = A$ and f_b for $X = B$ and exponent p can be modified based on the comparison of calculated and measured amplitude characteristics of non-rotating blades [17]. Components of slip velocity in ξ_x , η_x directions are given by time derivative of corresponding displacements in (19)

$$\begin{bmatrix} \dot{\xi}_X \\ \dot{\eta}_X \end{bmatrix} = \begin{bmatrix} \boldsymbol{\xi}_{X,C_j}^T & -\boldsymbol{\xi}_{X,D}^T \\ \boldsymbol{\eta}_{X,C_j}^T & -\boldsymbol{\eta}_{X,D}^T \end{bmatrix} \begin{bmatrix} \dot{\mathbf{q}}_{C_j} \\ \dot{\mathbf{q}}_D \end{bmatrix} \quad \text{for} \quad \begin{array}{l} X = A \wedge j = 2, \\ X = B \wedge j = 1. \end{array} \quad (28)$$

Transforming components of velocities and friction forces from coordinate spaces $\xi'_X \eta'_X$ to $\xi_X \eta_X$ leads to a term for friction forces in contact surfaces

$$\begin{bmatrix} T_{X\xi} \\ T_{X\eta} \end{bmatrix} = \boldsymbol{\tau}_X^T \mathbf{B}_X \boldsymbol{\tau}_X \begin{bmatrix} \boldsymbol{\xi}_{X,C_j}^T & -\boldsymbol{\xi}_{X,D}^T \\ \boldsymbol{\eta}_{X,C_j}^T & -\boldsymbol{\eta}_{X,D}^T \end{bmatrix} \begin{bmatrix} \dot{\mathbf{q}}_{C_j} \\ \dot{\mathbf{q}}_D \end{bmatrix} \quad \text{for} \quad \begin{array}{l} X = A \wedge j = 2, \\ X = B \wedge j = 1, \end{array} \quad (29)$$

where \mathbf{B}_X is diagonal matrix of equivalent damping given in (26) and $\boldsymbol{\tau}_X$ is transformation matrix

$$\boldsymbol{\tau}_X = \begin{bmatrix} \sin \delta_X & \sin \delta_X \\ -\sin \delta_X & \cos \delta_X \end{bmatrix}, \quad X = A, B. \quad (30)$$

Friction torque caused by relative rotation of the shroud with respect to friction element is expressed as

$$M_{X\zeta} = b_e(\phi_X, \omega_k) \left(\boldsymbol{\zeta}_X^T \dot{\boldsymbol{\varphi}}_{C_j} - \boldsymbol{\zeta}_x^T \dot{\boldsymbol{\varphi}}_D \right), \quad \begin{array}{l} (X = A \wedge j = 2 \wedge x = a) \quad \text{or} \\ (X = B \wedge j = 1 \wedge x = b), \end{array} \quad (31)$$

where coefficient of equivalent damping

$$b_e(\phi_X, \omega_k) = \frac{4 M_{X,0}}{\pi (\phi_X \omega_k)^p} \quad (32)$$

depends on friction torque $M_{X,0}$ and on amplitude of relative angular displacement

$$\phi_X = \left| \zeta_X^T \varphi_{C_j} - \zeta_x^T \varphi_D \right| \quad (33)$$

and transformation vectors have the form

$$\begin{aligned} \zeta_X^T &= [\mp \sin \delta_X, 0, \cos \delta_X], & \text{" - " for } X = A \wedge x = a, \\ \zeta_x^T &= [\mp \sin \delta_x, 0, \cos \delta_x], & \text{" + " for } X = B \wedge x = b. \end{aligned} \quad (34)$$

Acting of elastic and friction force effects in contact surfaces can be simultaneously expressed by force bivectors in contact points

$$\mathbf{f}_X = [T_{X\xi}, T_{X\eta}, N_X, M_{X\xi}, M_{X\eta}, M_{X\zeta}]^T, \quad X = A, B \quad (35)$$

expressing the effect of the shroud on friction element (see Fig. 1). Contact normal forces and torques N_X , $M_{X\xi}$, $M_{X\eta}$ are expressed by linearized contact stiffnesses at contact points $X = A, B$, expected area of effective contact surface, contact deformation in normal direction and relative angular displacements of the blade shroud with respect to the friction element around axes ξ_X and η_X as it has been described in section 2.

4. Case study

The methodology of the modelling presented above is used for dynamic analysis of a real blade couple. The blades are fixed to a rigid disk rotating with constant angular velocity. Detail geometrical description of the blades was gained from [17]. Based on the derived methodology, in-house software for computational blade modelling was developed. Using this software, each blade was discretized by six nodal points into five finite beam elements and the friction element is considered to be a rigid body with 6 DOF. The final computational model has then 78 DOF (two blades and one friction element).

4.1. Modal analysis

The linearized model (8) has been used as the first approximation of the nonlinear behaviour of the blade packet. Performing the modal analysis, we can see the influence of friction forces on the spectrum of eigenvalues. Let us note that the modal analysis is performed in following steps: Firstly, the steady state response to given excitation is calculated without the friction damping. Secondly, based on the gained steady state response the equivalent damping matrix is determined and consequently the modal analysis of the model including the equivalent damping is performed. Practically, it means that the modal properties depend on excitation frequency and amplitude.

Taking into account the influence of material, contact and friction damping, a certain number of complex eigenvalues vanishes and real eigenvalues appear instead. This is the desired positive effect of friction damping because the corresponding mode shapes are also super-critically damped. In this case, approximately 47 pairs of complex conjugate eigenvalues and 62 negative real eigenvalues appear. The number of complex and real eigenvalues changes slightly along with rotational speed of the disk. Further, because of the influence of matrices of gyroscopic effects, softening and bending stiffening under rotation and because of the coupling friction effects, imaginary parts of eigenvalues depend not only on rotational speed but also on excitation frequency. This effect can be clearly seen in Figs. 3 and 4, where

imaginary parts (natural frequencies) of the first fifteen (Fig. 3 left) and six (Fig. 3 right and Fig. 4) eigenvalues are plotted in dependence on rotational speed of the disk. The straight lines represent the excitation frequency. Mentioned figures have similar meaning as Campbell diagrams, i.e. intersections of straight lines and natural frequencies correspond to resonant states.

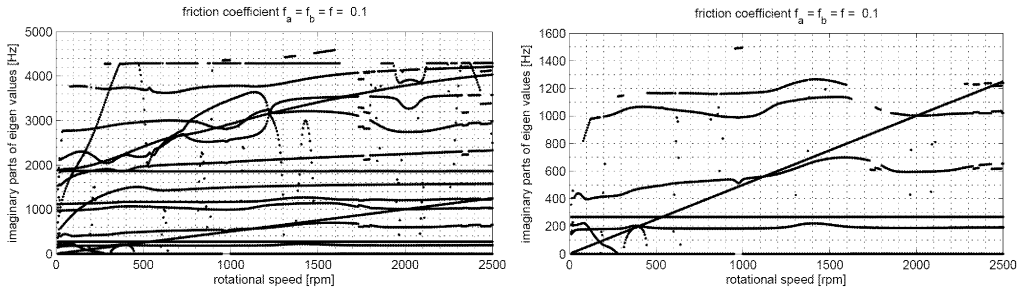


Fig.3: Dependence of imaginary parts of eigenvalues on rotational speed of the disk for excitation frequency $\omega_k = 30 \omega$ (left) and zoomed area corresponding to the first six eigenvalues (right)

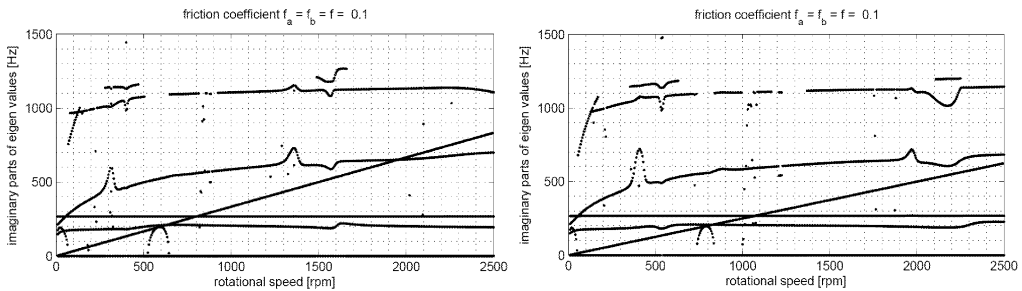


Fig.4: Dependence of imaginary parts of the first six eigenvalues on rotational speed of the disk for excitation frequency $\omega_k = 20 \omega$ (left) and $\omega_k = 15 \omega$ (right)

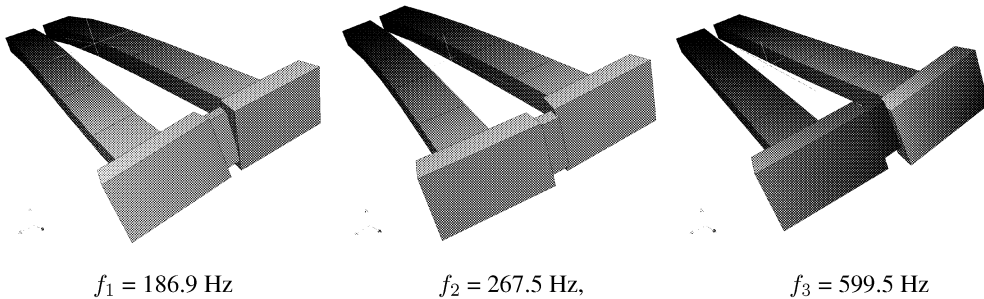


Fig.5: Representation of the first three complex mode shapes for 2000 rpm

To determine the significance of particular resonant state it is worthy to have notion of its mode shape and based on that the influence of the resonance can be judged. It can be clearly seen from following results that the first three resonances take effect only because centrifugal forces hinder slip motion for higher rotational speed. In Fig. 5, the complex mode shapes are displayed along with corresponding natural frequencies. The mode shapes have

been determined for 2000 rpm of the disk and for excitation frequency $\omega_k = 30\omega$, where the friction coefficient has been supposed to have value of $f = 0.1$.

4.2. Steady-state response to external nozzle excitation

The steady-state response is used for contact slip motion determination. The slip motion is supposed to have elliptical orbit and the aim is to investigate lengths of the major and the minor semi-axes of the ellipse. First, let us define the system parameters which primarily influence the blade motion. Slip properties of the contact surfaces are defined by friction coefficients $f_a = f_b = f$. The excitation defined in (10) is uniformly distributed along the blade, i.e. axial and tangential forces (11) act at each blade node. Amplitudes of the forces are inverse proportional to the multiple k of angular velocity ω , i.e. $F_t^{(k)} = F_t^{(1)}/k$ and $F_{ax}^{(k)} = F_{ax}^{(1)}/k$. As an illustration, let us consider three different excitations whose parameters are summarized in Table 1. The friction coefficient is chosen to be a variable parameter, which indicates the rate of friction forces in dependence on the contact surfaces properties.

k	$F_t^{(k)}$ [N]	$F_{ax}^{(k)}$ [N]
15	1.33	0.66
20	1	0.5
30	0.63	0.3

Tab.1: Definition of excitation parameters

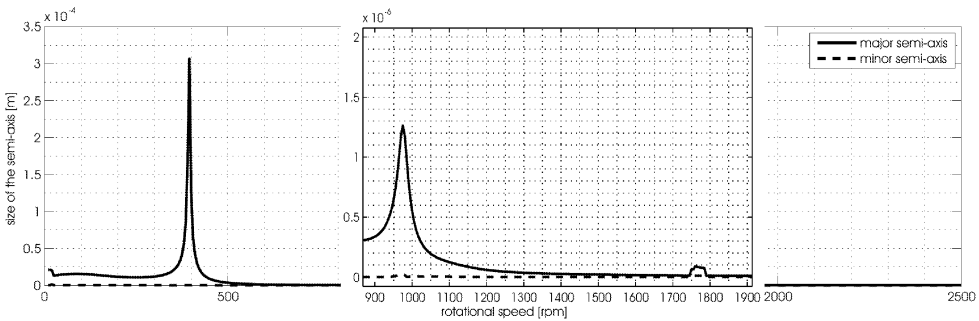


Fig.6: Length of semi-axes of elliptical orbit of contact point A for $\omega_k = 30\omega$

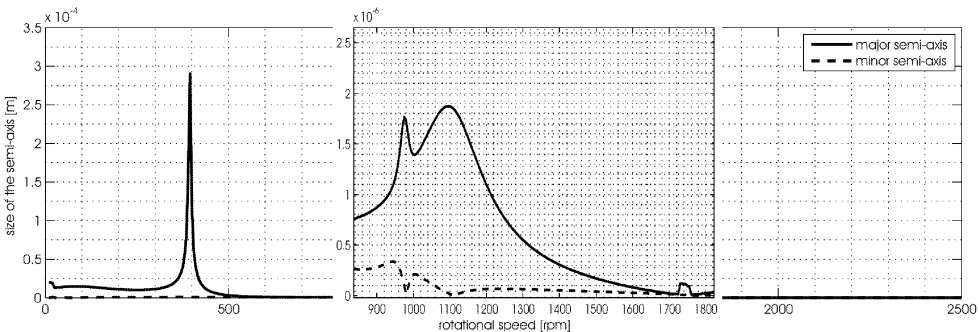


Fig.7: Length of semi-axes of elliptical orbit of contact point B for $\omega_k = 30\omega$

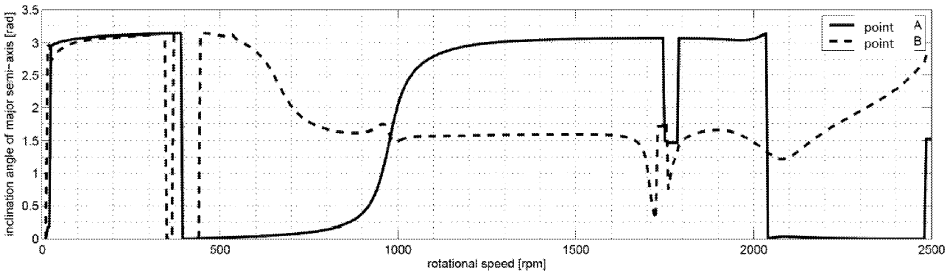


Fig.8: Inclination angles of major semi-axes of elliptical orbits for $\omega_k = 30 \omega$

Figs. 6 and 7 show the dependence of lengths of the major and the minor semi-axes of the elliptical orbits of contact points A and B on the rotational speed, respectively. One can clearly see that mainly the length of the major semi-axis is dominantly influenced by system vibration and by resonant states. In consequence of higher contact forces in surface a, which are proportional to square power of angular speed, the slip motion diminishes except the two resonant peaks. On the other hand, contact forces in surface b are smaller than in surface a and therefore the slip motion is much more influenced by the excitation and by the change of natural frequencies in dependence on rotational speed of the disk. One can see few resonant peaks in Fig. 7. The first one at $n = 390$ rpm corresponds to the resonance with the first natural frequency. The resonance with the second natural frequency has not been exhibited. The next two ones at $n = 975$ rpm and $n = 1130$ rpm correspond to the third natural frequency because the value of the third natural frequency changes along with the excitation and the straight line has two intersection with the third natural frequency. The fourth one is caused by a sudden jump of natural frequencies for $n = 1725$ rpm in Fig. 3. Fig.8 displays the dependance of inclination angles of major semi-axes with respect to axis ξ_A, ξ_B respectively.

Further, the friction coupling can be judged according to the dissipated energy amount by friction effects. Figs. 9–11 show dissipated energy by friction during one period of motion $T_k = 2\pi/\omega_k$ considering the steady state response of the linearized model (8). The dissipated energy amount is significant in the neighbourhood of the first resonant states only. Further, increasing the friction coefficient the dissipated energy increases too, except the resonant states, where the friction influences the dissipated energy amount in the range over the first

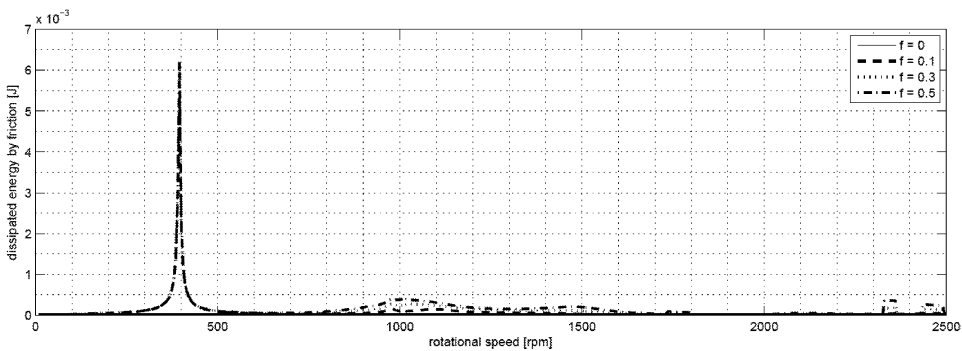


Fig.9: Total dissipated energy by friction in dependence on friction coefficient for $\omega_k = 30 \omega$

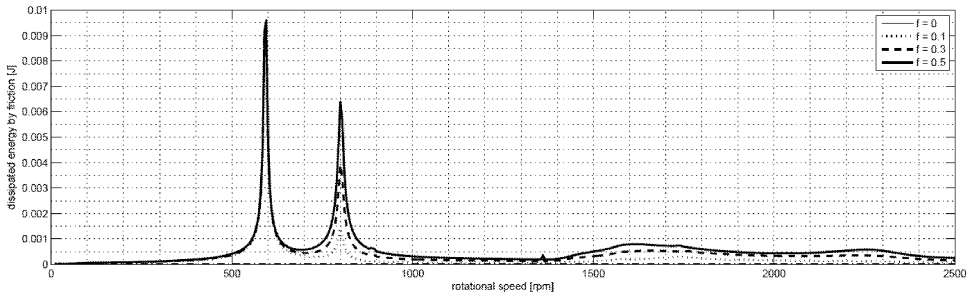


Fig.10: Total dissipated energy by friction in dependence on friction coefficient for $\omega_k = 20 \omega$

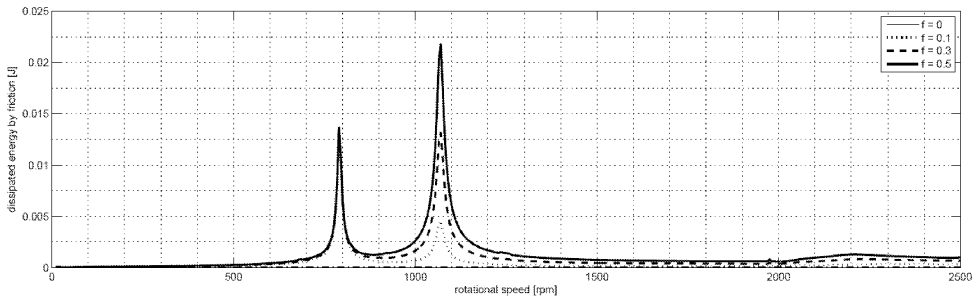


Fig.11: Total dissipated energy by friction in dependence on friction coefficient for $\omega_k = 15 \omega$

resonance. According to Figs.10 and 11 it can be observed that decreasing the multiple k in the excitation frequency, the contribution of the first resonance to the dissipation energy diminishes and the energy is dissipated more by the second resonance.

To have a clear idea about the friction element motion in between the shroud, we can plot the elliptical orbits of both contact points A and B . Fig.12 shows elliptical orbits of contact points for the excitation $F^{(30)}$, $k = 30$ defined in Tab.1. Unlike the dissipation energy amount, the elliptical orbit reduces in size while increasing the friction coefficient and moreover the inclination angle tends to be $\pi/2$ for higher values of friction coefficients. The lengths of semi-axes of the ellipse agree with micro slip motion. The difference between the two ellipses originates from the different inclinations of the surfaces with respect to the blade centre line.

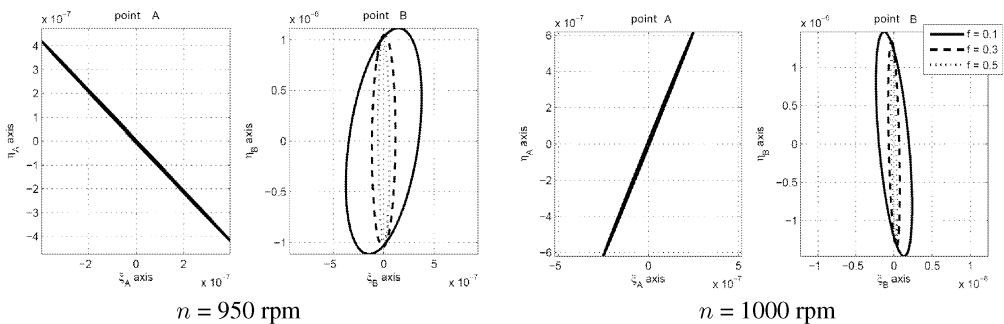


Fig.12: Elliptical orbits of contact points A and B for $\omega_k = 30 \omega$

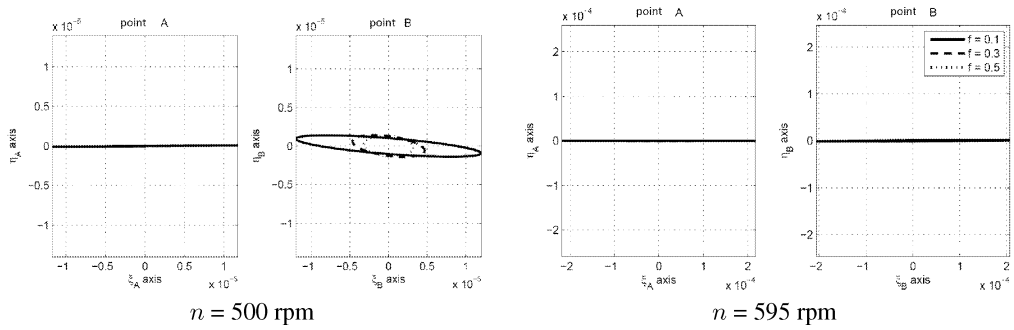


Fig.13: Elliptical orbits of contact points in surfaces A and B for $\omega_k = 20 \omega$

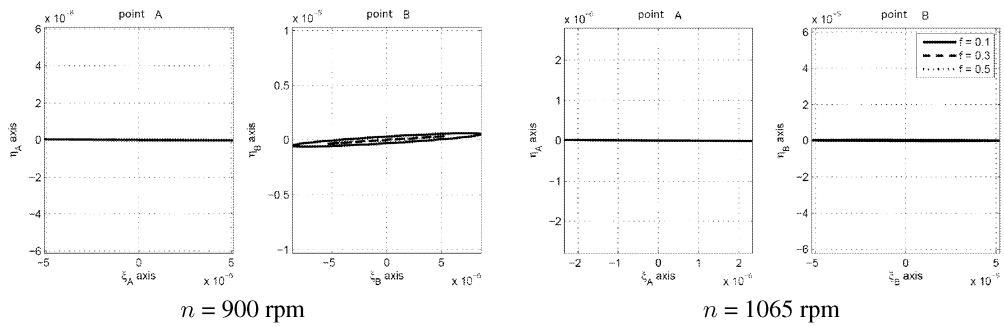


Fig.14: Elliptical orbits of contact points in surfaces A and B for $\omega_k = 15 \omega$

In case of Fig. 13 we can observe the orbits of contact points for pre-resonant state at $n = 500$ rpm and for resonant state at $n = 595$ rpm for the second excitation. Similarly, orbits of contact points in Fig. 14 correspond to two different operational states.

5. Conclusions

This paper presents a method focused on the modelling of friction effects in the blade shroud, which are realized by means of friction elements placed in between the blade shroud. A model of two rotating blades with shroud is used. Friction forces and torques are linearized using the harmonic balance method under assumption, that the contact points move approximately along the ellipses. Based on this, equivalent damping coefficients are determined in dependence on the lengths of semi-axes of the ellipse defining the slip motion between blades and the friction element. Using the linearized model of two blades with friction element, modal analysis was performed and the dissipation energy amount by friction together with the elliptical orbits were investigated for different excitation frequencies. According to the methodology the in-house software in MATLAB was created and tested on the model of two rotating blades with shroud.

Acknowledgement

This work was supported by the research project MSM 4977751303 of the Ministry of Education, Youth and Sports and by GA CR project No. 101/09/1166 ‘Research of dynamic behaviour and optimization of complex rotating systems with non-linear couplings and high damping materials’.

References

- [1] Cigeroğlu E., An N., Menq C.H.: A microslip friction model with normal load variation induced by normal motion, *Nonlinear Dynamics* 50 (2007) 609–626
- [2] Allara M.: A model for the characterization of friction contacts in turbine blades, *Journal of Sound and Vibration* 320 (2009) 527–544
- [3] Firrone C.M., Zucca S.: Underplatform dampers for turbine blades: The effect of damper static balance on the blade dynamics, *Mechanics Research Communications* 36 (2009) 515–522
- [4] Borrajo J.M., Zucca S., Gola M.M.: Analytical formulation of the Jacobian matrix for non-linear calculation of forced response of turbine blade assemblies with wedge friction dampers, *International Journal of Non-Linear Mechanics* 41 (2006) 1118–1127
- [5] Csaba G.: Forced response analysis in time and frequency domains of a tuned bladed disk with friction dampers, *Journal of Sound and Vibration* 214 (3) (1998) 395–412
- [6] Cigeroğlu E., Özgüven H. N.: Nonlinear vibration analysis of bladed disks with dry friction dampers, *Journal of Sound and Vibration* 295 (2006) 1028–1043
- [7] Cha D., Sinha A.: Statistics of responses of a mistuned and frictionally damped bladed disk assembly subjected to white noise and narrow band excitations, *Probabilistic Engineering Mechanics* 21 (2006) 384–396
- [8] Brepta R., Půst L., Turek F.: *Mechanické kmitání*, Sobotáles, Praha 1994
- [9] Toufine A., Barrau J.J., Berthillier M.: Dynamics study of a structure with flexion-torsion coupling in the presence of dry friction, *Nonlinear Dynamics* 18 (1999) 321–337
- [10] Tokar I.G., Zinkovskii A.P., Matveev V.V.: On the problem of improvement of the damping ability of rotor blades of contemporary gas-turbine engines, *Strength of Materials* 35 (4) (2003) 368–375
- [11] Schmidt-Fellner A., Siewert C., Panning L.: Experimental analysis of shrouded blades with friction contact, *Proceedings in Applied Mathematics and Mechanics* 6 (2006) 263–264
- [12] Bigret R.: *Blades nad bladed disks*, Encyclopedia of Vibration, Vol. 1, Editor-in Chief Braoun S., Accademic Press, London, San Diego, 2001
- [13] Kellner J.: *Kmitání turbínových lopatek a olopatkovaných disků*, Disertační práce, ZČU v Plzni, 2009 (in Czech)
- [14] Míšek T., Tetiva A., Prchlík L., Duchek K.: Prediction of High Cycle Fatigue Life of Steam Turbine Blading Based on Unsteady CFD and FEM Forced Response Calculation, *Proceedings of the ASME Turbo Expo 2007*, Montreal 2007
- [15] Rivin E.I.: *Stiffness and Damping in Mechanical Design*, Marcel Dekker, New York, 1989
- [16] Sextro W.: *Dynamical Contact Problems with Friction*, Springer, Berlin, Heidelberg, 2007
- [17] Půst L., Horáček J., Radolfová A.: *Kmitání nosíku s třecí ploškou na kolmých nástavcích*, Ústav termomechaniky AVČR, Praha, 2008 (in Czech)

Received in editor's office: March 23, 2010

Approved for publishing: August 24, 2010

Note: This paper is an extended version of the contribution presented at the national colloquium with international participation *Dynamics of Machines 2010* in Prague.